Operator evolution for *ab initio* electric dipole transitions of ^{4}He

Micah D. Schuster,[1,*] Sofia Quaglioni,[2,†] Calvin W. Johnson,[1,‡] Eric D. Jurgenson,[2] and Petr Navrátil[3]
[1]*San Diego State University, 5500 Campanile Drive, San Diego, California 92182, USA*
[2]*Lawrence Livermore National Laboratory, P.O. Box 808, L-414, Livermore, California 94551, USA*
[3]*TRIUMF, 4004 Wesbrook Mall, Vancouver, British Columbia, Canada, V6T 2A3*
(Received 2 April 2015; revised manuscript received 29 May 2015; published 24 July 2015)

A goal of nuclear theory is to make quantitative predictions of low-energy nuclear observables starting from accurate microscopic internucleon forces. A major element of such an effort is applying unitary transformations to soften the nuclear Hamiltonian and hence accelerate the convergence of *ab initio* calculations as a function of the model space size. The consistent simultaneous transformation of external operators, however, has been overlooked in applications of the theory, particularly for nonscalar transitions. We study the evolution of the electric dipole operator in the framework of the similarity renormalization group method and apply the renormalized matrix elements to the calculation of the ^{4}He total photoabsorption cross section and electric dipole polarizability. All observables are calculated within the *ab initio* no-core shell model. We find that, although seemingly small, the effects of evolved operators on the photoabsorption cross section are comparable in magnitude to the correction produced by including the chiral three-nucleon force and cannot be neglected.

DOI: 10.1103/PhysRevC.92.014320 PACS number(s): 21.60.De, 05.10.Cc, 23.20.Js, 27.10.+h

I. INTRODUCTION

Unitary transformations of the Hamiltonian have been used to great effect in a range of nuclear physics problems [1–11] to decouple high- and low-momentum components of the interaction and promote numerical convergence in large, but finite model spaces. However, in an A-nucleon system, such beneficial decoupling of momentum scales comes at the price of an effective Hamiltonian containing irreducible three- and higher-body (up to A-body) terms, even when initially absent. In addition, for consistency the same unitary transformation must to be applied to any operator associated with measurable quantities. This, once again, will induce many-body operators.

Widely adopted is the similarity renormalization group (SRG) method, which employs a continuous unitary transformation of the Hamiltonian characterized by a momentum resolution scale λ [12]. The SRG transformation (or evolution) of the Hamiltonian has been carried out up to the three-body level both on a harmonic oscillator (HO) basis [8,13–15] and, more recently, in momentum representation [16], and the resulting interactions have been successfully applied to compute properties of a variety of nuclei [8,9,11,13,14,17–19].

For systems with up to $A \simeq 10$ nucleons, bound-state calculations including up to three-body-induced forces have been shown to lead to energies mostly independent of λ above 1.8 fm^{-1}, i.e., to approximately preserve the unitarity of the transformation [8,13,14]. Small variations of the SRG momentum scale around 2 fm^{-1} have been also shown to produce mostly negligible differences in n-^{4}He [20] and n-^{8}Be [21] elastic phase shifts, but a more quantitative investigation has not been possible due to a slower rate of convergence for larger λ values combined with the high computational demand.

Few studies have dealt with the consistent transformation and application of operators, the other component required for an accurate description of measurable nuclear properties when using effective interactions. This was first studied using the Okubo-Lee-Suzuki (LS) renormalization [1,22,23] to compute electromagnetic properties for several nuclei [24]. For the SRG, the evolution of operators was achieved for the first time in the deuteron, where only one- or two-body operators are relevant, working in a momentum representation [25]. The more complicated process of evolving and applying operators in finite nuclei beyond the deuteron was first examined in Ref. [26]. There, working on a translationally invariant HO basis, we extended the approach of Ref. [13] to evolve scalar (i.e., rank zero in both angular momentum and isospin) operators in the two- and three-body spaces and used the resulting matrix elements to calculate expectation values on the ground state (g.s.) of the ^{4}He nucleus. (Note that only scalar operators contribute to expectation values for this $J^\pi T = 0^+0$ four-nucleon state.) In particular, we showed that the inclusion of up to three-body matrix elements in the ^{4}He nucleus all but completely restores the invariance of the root-mean square radius and total electric dipole strength under the SRG transformation.

While the work of Ref. [26] allowed us to perform initial proof-of-principle calculations, a general description of observables also requires the ability to evolve, and embed in finite nuclei, nonscalar operators. Further, more work is needed to accurately assess the consistency of the SRG approach for the description of continuum observables. Starting from an initial nucleon-nucleon plus three-nucleon ($NN + 3N$) Hamiltonian from chiral effective field theory [27,28], in this paper we present the first application of the SRG approach to compute the ^{4}He photoabsorption cross section and electric dipole polarizability. All induced forces up to the three-body level are retained in the transformed Hamiltonian, while the leading electric dipole transition operator is determined (for the first time) by evolution in the $A = 2$ system. All

*mschuste@rohan.sdsu.edu
†quaglioni1@llnl.gov
‡cjohnson@mail.sdsu.edu

calculations are performed within the *ab initio* no-core shell model (NCSM) [29] working with translationally invariant HO basis states. The photoabsorption cross section is computed by means of the Lorentz integral transform (LIT) method [30,31], while the electric polarizability is obtained according to Podolsky's technique [32]. This allows us to bypass the direct calculation of scattering states and to work only with square-integrable basis states.

An *ab initio* investigation of both the photoabsorption cross section [33] and the electric polarizability [34] of the ^{4}He nucleus based on chiral $NN + 3N$ interactions had already been accomplished in the past using LS effective interactions at the three-body cluster level [35,36], albeit without renormalization of the electric dipole operator. The primary purpose of the present work is to use these observables as testing grounds to explore the performance and consistency of the SRG approach. In particular we perform the first accurate investigation of the dependence on the SRG momentum scale of a continuum observable within a large range of λ values.

The paper is organized as follows. Section II provides background on the formalism adopted. In particular, we discuss how the SRG method modifies the Hamiltonian and external operators and how the LIT can be used to compute the response induced by an external perturbation, in our case, the dipole operator. In Sec. III we describe our results in three parts: convergence of the observables computed with respect to the size of the NCSM model space adopted, a discussion on the unitarity of the SRG transformation in our context, and a comparison to experimental cross section data. Lastly, Sec. IV gives a brief summary of our results and describes the next steps in this research.

II. BACKGROUND

A. Hamiltonian and spectral resolution method

We start with the intrinsic nonrelativistic Hamiltonian for a system of A nucleons (protons and neutrons):

$$\hat{H} = \frac{1}{A}\sum_{i<j}\frac{(\vec{p}_i - \vec{p}_j)^2}{2M_N} + \sum_{i>j}^{A} V_{ij}^{NN} + \sum_{i>j>k}^{A} V_{ijk}^{3N}, \quad (1)$$

where V_{ij}^{NN} and V_{ijk}^{3N} are, respectively, two- and three-nucleon free-space interactions, which depend on the relative coordinates (and/or momenta for nonlocal forces) between particles; $\vec{p}_i$ is the momentum of particle i; and M_N is the nucleon mass. We then look for the eigenfunctions of $\hat{H}$ in the form of expansions over a complete set of translationally invariant and fully antisymmetric A-body states. This amounts to diagonalizing the Hamiltonian in the many-body basis. In particular, we use the Jacobi-coordinate HO basis of the *ab initio* NCSM [29], in which the model space is defined by all A-body states up to a maximum excitation of $N_{\max}\hbar\Omega$ above the minimum energy configuration of the system and Ω is the HO frequency.

While in principle the above is an exact prescription for the solution of the Schrödinger equation associated with the Hamiltonian of Eq. (1), in practice we work with a finite model space and achieve convergence to the exact results with increasing $N_{\max}$. Crucial for the success of this approach is the use of unitary transformations of the Hamiltonian chosen to reduce the coupling between high- and low-momentum states, which arises from the strong short-range repulsion of the bare nuclear interaction and leads to slow convergence in the size of the model space. Here we focus on the unitary transformation described by the SRG approach outlined in the next section.

Our numerical method of choice for obtaining the spectrum of energy states of the Hamiltonian is the Lanczos method [37]. Given a starting arbitrary unit vector $|\phi_0\rangle$, it recursively allows us to define a set of orthonormal basis states $|\phi_i\rangle$—known as Lanczos vectors—for which the Hamiltonian matrix assumes a tridiagonal form:

$$b_{i+1}|\phi_{i+1}\rangle = \hat{H}|\phi_i\rangle - a_i|\phi_i\rangle - b_i|\phi_{i-1}\rangle. \quad (2)$$

Here $|\phi_{-1}\rangle = 0$, and $a_i = \langle\phi_i|\hat{H}|\phi_i\rangle$ and $b_i = \||b_i|\phi_i\rangle\|$ are, respectively, the diagonal and upper (lower) diagonal elements of the Hamiltonian in the new basis, or Lanczos coefficients as they are often called. The power of the Lanczos method is that the extremum eigenvalues of the Hamiltonian quickly converge to their true value after a limited number of iterations, much smaller than the dimension of the problem. Further, relevant to the calculation of the ^{4}He photoabsorption cross section and electric polarizability discussed in this paper, the Lanczos coefficients can be used to accurately evaluate the expectation value of the Green's function on a normalized vector, $G(z) = \langle\phi_0|(z - \hat{H})^{-1}|\phi_0\rangle$, in terms of the continued fraction [38,39]

$$G(z) = \cfrac{1}{z - a_0 - \cfrac{b_1^2}{z - a_1 - \cfrac{b_2^2}{z - a_2 - \cfrac{b_3^2}{\ddots}}}}. \quad (3)$$

B. SRG evolution

As implemented for nuclear physics [12,40], the SRG method employs a unitary transformation, U_s, on the initial Hamiltonian $\hat{H}_{s=0} = \hat{H}$,

$$\hat{H}_s = \hat{U}_s\hat{H}_{s=0}\hat{U}_s^\dagger, \quad (4)$$

that can be implemented as a flow equation [41] in the continuous parameter s and an anti-Hermitian generator $\hat{\eta}_s = (d\hat{U}_s/ds)\hat{U}_s^\dagger$,

$$\frac{d\hat{H}_s}{ds} = [\hat{\eta}_s, \hat{H}_s]. \quad (5)$$

Although other generators have been used [15,42], a common choice for this operator is the commutator of the evolved Hamiltonian with the kinetic energy, $\hat{\eta}_s = [\hat{T}, \hat{H}_s]$. This drives the Hamiltonian towards a diagonal form in momentum space, thus decoupling high- and low-momentum states. The spread of the residual off-diagonal strength can be measured by the parameter with units of momentum λ [where $s^{-1} = (\hbar\lambda)^4/M_N^2$], which can be used to follow the evolution of the Hamiltonian in place of s. As λ decreases, the Hamiltonian undergoes more evolution while $\lambda = \infty$ corresponds to the initial Hamiltonian.

Working within a discrete basis, Eq. (5) can be cast into a set of coupled first-order differential equations for the matrix elements of the flowing Hamiltonian $\hat{H}_s$, with the right-hand side of the equation being simply given by matrix multiplications. The procedure to determine the two- and three-body components of the evolved Hamiltonian within the Jacobi-coordinate HO wave functions adopted in this work is presented in Refs. [8,13]. In particular, depending on the absence or presence of V^{3N} in Eq. (1), one can identify three classes of evolved Hamiltonians: (1) NN-only, two-body Hamiltonian from the SRG evolution of the NN force in the two-nucleon space; (2) $NN + 3N$-induced, three-body Hamiltonian from the SRG evolution of the NN force in the $3N$ space; and (3) $NN + 3N$, SRG Hamiltonian obtained from evolving the NN plus initial $3N$ force in the $3N$ system.

The consistent application of the SRG approach requires that any other operator, $\hat{O}$, undergo the same unitary transformation as the Hamiltonian, i.e.,

$$\hat{O}_s = \hat{U}_s \hat{O}_{s=0} \hat{U}_s^\dagger. \tag{6}$$

While this can be rewritten into a form similar to Eq. (5), it is more computationally efficient to compute the unitary transformation, $\hat{U}_s$, using the eigenvectors of the Hamiltonian before and after the transformation, $|\psi_\alpha(0)\rangle$ and $|\psi_\alpha(s)\rangle$, respectively,

$$\hat{U}_s = \sum_\alpha |\psi_\alpha(s)\rangle\langle\psi_\alpha(0)|. \tag{7}$$

In a discrete basis, the transformation of Eq. (6) is then given, once again, by simple matrix multiplications. In particular, for parity-conserving rank-zero operators (as for the Hamiltonian, working in the isospin formalism) $\hat{U}_s$ corresponds to a block-diagonal matrix with respect to the various angular-momentum, parity, and isospin channels ($J^\pi T$) of the system, and the evolution can be performed block by block in parallel with that of $\hat{H}_s$. This type of evolution for operators, in both the $A = 2$ and $A = 3$ systems, has been recently implemented working within the Jabobi-coordinate NCSM basis [26]. The situation is more complicated for nonscalar operators, as they will couple different blocks. In this case, the unitary transformation must be computed and stored for each block during the evolution of the Hamiltonian and the matrix elements of the evolved operator must be reconstructed in a second step. In this work, we have implemented this process in the $A = 2$ space, while we defer to future work the technically more challenging process of evolving nonscalar operators in the three-body space.

In general, to determine the two- and three-body components of an evolved operator we follow a procedure similar to that adopted for the Hamiltonian in Refs. [8,13]. We start by evolving $\hat{H}_s$, hence calculating $\hat{U}_s$, in the $A = 2$ system and determining the matrix elements of the two-body evolved operator, $\langle\hat{O}_s^{(2)}\rangle$, through Eq. (6). Next, (for scalar operators) we repeat the operation in the $A = 3$ system, thus computing $\langle\hat{O}_s^{(3)}\rangle$, and then isolate the induced three-body components of the evolved operator via subtraction, $\langle\hat{O}_s^{(3)}\rangle - \langle\hat{O}_s^{(2)}\rangle$, where the second term corresponds to the two-body evolved operator embedded in the $3N$ basis. This allows us to accurately calculate and separate the two- and three-body matrix elements of the evolved operator, which we can then use unchanged in calculations for any nucleus. The second step can also be performed with or without the initial $3N$ force in the Hamiltonian. Similar (but not quite parallel) to the three classes of Hamiltonian discussed earlier, this procedure leads to the following three stages of operator evolution: (1) bare or unevolved operator; (2) two-body (2B) evolved, SRG evolution of the operator in the 2B space; and (3) three-body (3B) evolved, SRG evolution of the operator in the 3B space, allowing the induction of 3B terms.

C. Photoabsorption cross section and electric polarizability

At low excitation energies, when the long-wavelength limit applies, the nuclear photoabsorption process can be described by the cross section [43]

$$\sigma_\gamma(\omega) = 4\pi^2 \frac{e^2}{\hbar c} \omega R(\omega), \tag{8}$$

where ω is the perturbing photon energy and $R(\omega)$ is the inclusive response function, given by

$$R(\omega) = \int d\Psi_f |\langle\Psi_f|\hat{D}|\Psi_0\rangle|^2 \delta(E_f - E_0 - \omega), \tag{9}$$

where E_f and E_0 represent the final-state and g.s. energies along with their associated wave functions, $|\Psi_f\rangle$ and $|\Psi_0\rangle$, respectively, and $\hat{D}$ is the electric dipole operator,

$$\hat{D} = \sqrt{\frac{4\pi}{3}} \sum_{i=1}^{A} \frac{\tau_i^z}{2} r_i Y_{10}(\hat{r}_i). \tag{10}$$

Here, τ_i^z is the third component of isospin and $\vec{r}_i = r_i \hat{r}_i$ is the position vector of the ith particle in the center-of-mass frame.

To bypass the direct calculation of the final states, which for a light nucleus such as ^{4}He are all in the energy continuum, the LIT method [30,31] obtains the response function, $R(\omega)$, after the evaluation and subsequent inversion [44,45] of its convolution with a Lorentzian kernel of finite width σ_I,

$$L(\sigma_R,\sigma_I) = \int d\omega \frac{R(\omega)}{(\omega - \sigma_R)^2 + \sigma_I^2}, \tag{11}$$

where σ_R is a continuous variable with unit of energy. Taking advantage of the completeness of the eigenstates of the Hamiltonian this can be rewritten as [46]

$$L(\sigma_R,\sigma_I) = -\frac{M_0}{\sigma_I} \mathrm{Im}\{G(z)\}, \tag{12}$$

where $G(z)$ is the Green's function of Eq. (3) evaluated at the complex energy $z = E_0 + \sigma_R + i\sigma_I$ on the starting Lanczos vector $|\phi_0\rangle = M_0^{-1/2} \hat{D}|\Psi_0\rangle$. The quantity M_0 is the total strength of the transition induced by the dipole operator, which can be evaluated either directly as the expectation value $M_0 = \langle\Psi_0|\hat{D}^\dagger\hat{D}|\Psi_0\rangle$ of the operator $\hat{D}^\dagger\hat{D}$ on the g.s. wave function or as the square norm $M_0 = ||\hat{D}|\Psi_0\rangle||^2$ of the vector $\hat{D}|\Psi_0\rangle$. In the first case, only the scalar component of the $\hat{D}^\dagger\hat{D}$ operator is needed for the evaluation of the total dipole strength on the $J^\pi T = 0^+0$ g.s. of the ^{4}He nucleus.

Similarly, in the unretarded dipole long-wavelength approximation adopted here, the electric dipole polarizability of the

nucleus is given by

$$\alpha_E = 2\frac{e^2}{\hbar c}\int d\Psi_f \frac{|\langle\Psi_f|\hat{D}|\Psi_0\rangle|^2}{E_f - E_0}, \tag{13}$$

which corresponds to the double inverse-energy weighted sum rule of the photoabsorption cross section of Eq. (8):

$$\alpha_E = \frac{1}{2\pi^2}\int_{\omega_{\rm th}}^{\infty} d\omega \frac{\sigma_\gamma(\omega)}{\omega^2}, \tag{14}$$

with $\omega_{\rm th}$ being the threshold energy for photoabsorption. While the electric polarizability can be obtained through Eq. (14) by numerical integration of the computed cross section of Eq. (8), it is more efficient and numerically more accurate to take advantage of the completeness of the eigenstates of the Hamiltonian and directly evaluate it by means of the Lanczos method as

$$\alpha_E = -2\frac{e^2}{\hbar c} M_0 G(E_0), \tag{15}$$

with the same starting vector as in Eq. (12).

III. RESULTS

All results are obtained employing the Idaho N^{3}LO nucleon-nucleon interaction of Ref. [47] and the N^{2}LO 3N force from Ref. [48] with the low-energy constants adjusted to reproduce the triton half-life and the binding energies of ^{3}H and ^{3}He nuclei [49]. Unless otherwise stated, we truncate all of our calculations in the $A = 2$ model space at $N_{\rm max} = 300$ and in the $A = 3$ model space at $N_{\rm max} = 40$, denoted as $N_{A2\rm max}$ and $N_{A3\rm max}$, respectively. The HO model-space size for the ^{4}He system is simply indicated as $N_{\rm max}$.

In Sec. III A we start by exploring the evolution of a few matrix elements of the dipole transition. Next, in Sec. III B, we discuss the convergence properties of our results with respect to variations in both $N_{\rm max}$ and HO frequency, $\hbar\Omega$. Finally, in Sec. III C, we study the λ dependence of our calculations, and in Sec. III D we present a comparison with available experimental data.

A. Two-body evolved dipole operator

To obtain the photoabsorption cross section and electric dipole polarizability of Sec. II C within the SRG approach, we need to consider the evolution of the electric dipole operator of Eq. (10) that induces a $J^\pi T = 1^- 1$ transition between the initial and final states. For ^{4}He, the total dipole strength entering Eqs. (12) and (15) can be evaluated as the expectation value of a scalar operator, and we can use the technology we developed in Ref. [26] to renormalize $\hat{D}^\dagger\hat{D}$ (a scalar operator) up to the 3B level. However, the matrix elements of $\hat{D}$ are still needed to compute the Lanczos starting vector, which is proportional to $\hat{D}|\Psi_0\rangle$. As already mentioned in Sec. II B, properly evolving a nonscalar operator introduces additional technical complications, particularly in the $A = 3$ system. At the same time, we expect that the renormalization of the dipole will principally affect the total strength M_0 and have a relatively smaller effect on the Green's functions $G(z)$ and $G(E_0)$ of Eqs. (12) and (15), respectively, which are mainly driven by the energy spectrum of the system. If the Hamiltonian is evolved up to the 3B level, such a spectrum is also mostly independent from the SRG momentum scale. Therefore, for the time being we limit ourselves to 2B matrix elements of the evolved $\hat{D}$ in the calculation of the Lanczos starting vector.

Figure 1 shows snapshots of the evolution of the dipole operator in HO space for $^3S_1$ ($T = 0$) to $^3P_2$ ($T = 1$) transitions. The color bar represents the value of HO matrix elements and is truncated to highlight the off-diagonal behavior as the operator is evolved. Because this is a transition between different initial and final states, the representation in the HO space is not symmetric. Snapshots of this kind are useful for examining the behavior of the matrix elements during evolution and have been shown previously for operators evolved in momentum space [25] and for the Hamiltonian evolved in the HO [15,50] and momentum space [12,51]. Here, the discretized axes, n and n', are the radial quantum numbers of the HO wave function and directly correspond to the energy in HO space. For this transition, the bare operator starts as a lower bidiagonal matrix and as λ decreases we see increased strength in the off-diagonal matrix elements. So while the SRG evolves the momentum space Hamiltonian to a more diagonal form, it spreads out the dipole operator in HO space.

B. Convergence

In this section, we discuss the behavior of our calculations with respect to variations of the frequency $\hbar\Omega$ and the size $N_{\rm max}$ of the adopted HO model space. We start in Fig. 2 by

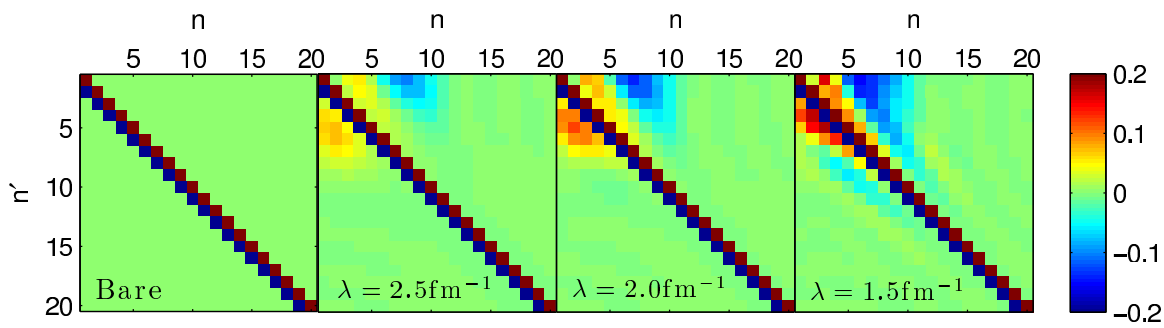

FIG. 1. (Color online) SRG evolution of the 2B dipole operator in HO space for the $^3S_1$ to $^3P_2$ transition. The color bar represents the value of the dipole matrix elements and is truncated to highlight the off-diagonal behavior as a function of evolution, from bare ($\lambda = \infty$) to $\lambda = 1.5$ fm^{-1}. The matrix elements have units of femtometers.

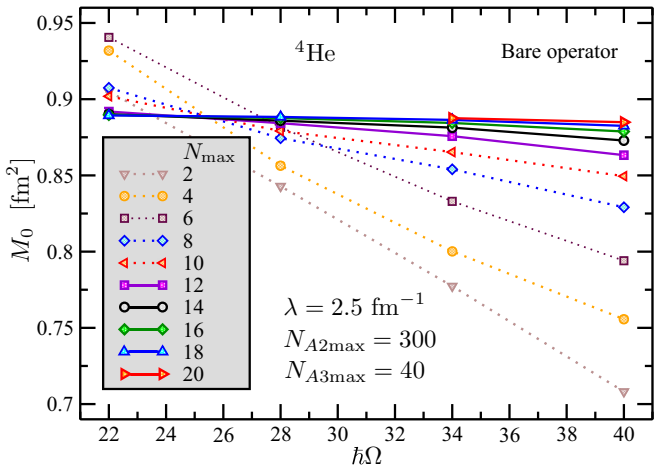

FIG. 2. (Color online) Convergence of the total dipole strength M_0 of ^{4}He as a function of $N_{\max}$ using the bare operator and evolved wave functions from the $NN + 3N$ Hamiltonian with $\lambda = 2.5$ fm^{-1} at $\hbar\Omega = 22$, 28, 34, and 40 MeV.

analyzing the total strength, M_0, of the bare dipole operator evaluated on the ^{4}He evolved g.s. wave function (using, in this example, the $NN + 3N$ Hamiltonian with $\lambda = 2.5$ fm^{-1}) for a range of HO frequencies and various basis sizes. As $N_{\max}$ increases, the total dipole strength becomes more and more independent from the choice of the $\hbar\Omega$ value in the range 22–40 MeV, reaching a flat behavior in the largest model spaces. The weakest $N_{\max}$ dependence is found for frequencies between 22 and 28 MeV, for which an excellent convergence is already achieved at $N_{\max} = 18$ proceeding from above and from below, respectively. These two $\hbar\Omega$ values are adopted for the reminder of our study. In addition, our choices for $N_{\max}$ have been shown to be fully converged and robust against changes to the HO frequency [52].

The typical convergence of M_0 as a function of $N_{\max}$, computed as the norm $||\hat{D}|\Psi_0\rangle||^2$, for the bare and 2B evolved dipole operators is presented in Figs. 3(a) and 3(b), respectively. Because the dipole is a long-range operator, we see almost no increase in the rate of convergence of the evolved over the bare operator (both evaluated, as in Fig. 2, on $NN + 3N$ evolved wave functions). Rather, the SRG evolution of the wave function provides a smooth convergence pattern, especially at smaller values of λ, regardless of the level of operator evolution. As an example, for $\lambda = 2.5$ fm^{-1} the M_0 values begin to follow an exponential convergence above $N_{\max} = 10$, whereas at $\lambda = 1.8$ fm^{-1} the exponential convergence already starts at $N_{\max} \sim 6$. This could be used effectively to extrapolate to $N_{\max} = \infty$ in heavier systems where one cannot feasibly reach large $N_{\max}$ values or where convergence of observables is very slow.

As is discussed in the next section and can be seen in Figs. 3(a) and 3(b), for dipole transitions the converged values tend to increase as λ decreases. This is due to the omission of induced many-body [3B and four-body (4B) in the case of Fig. 3(b)] contributions to the SRG evolved operator. Indeed, the difference between the M_0 values obtained with bare and 2B evolved operators is much larger at 1.8 than at 3.0 fm^{-1} due to the increasing strength of the SRG-induced terms as λ decreases.

In Fig. 4 we compare the convergence with respect to $N_{\max}$ of M_0 computed in two different ways: as the norm $||\hat{D}|\Psi_0\rangle||^2$ of the 2B evolved dipole operator, $\hat{D}$, acting on the ^{4}He g.s. and as the expectation value on the g.s. wave function of the 2B evolved $\hat{D}^\dagger\hat{D}$ operator. The two procedures yield the same results when the bare operators are employed, represented by the arrow in the figure. However, in general the same is not true upon the SRG evolution, which results in slightly different M_0 values. There are two factors that contribute to this difference: (i) the operators exhibit different short-range properties (in this case, r versus r^2, respectively); and (ii) in calculating M_0 as the square norm of the 2B evolved dipole operator acting on the ground state, we also implicitly include selected 3B and 4B matrix elements. Similar to what we have observed for the bare operator, varying the oscillator frequency from 22 to 28 MeV produces little change in the converged value of the observables. This is not surprising considering the large model

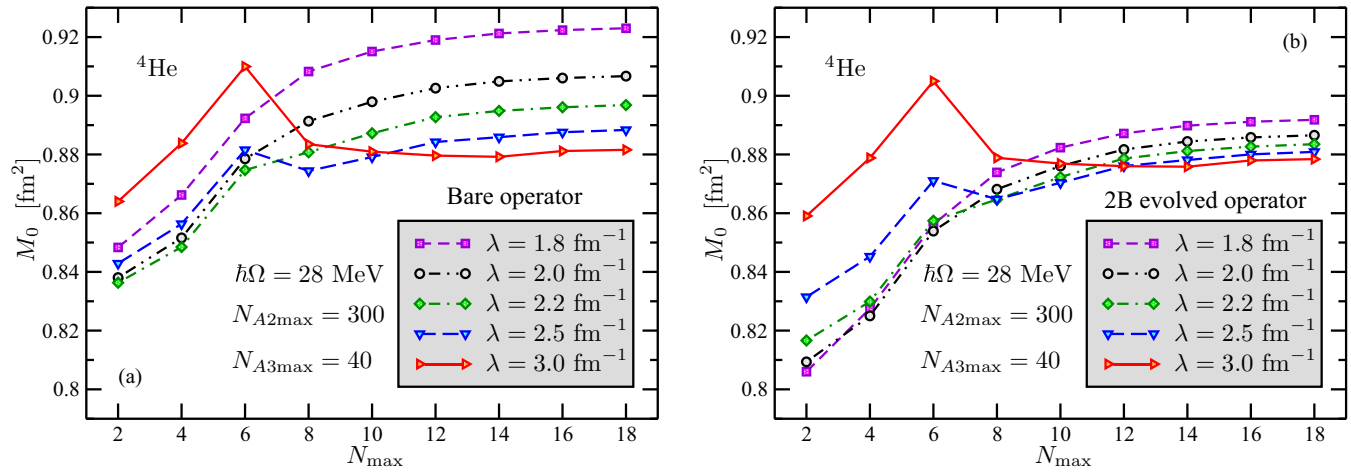

FIG. 3. (Color online) Convergence of the total dipole strength M_0 of ^{4}He as a function of $N_{\max}$ at $\hbar\Omega = 28$ MeV using (a) the bare and (b) the 2B evolved $\hat{D}$ operator and wave functions from the $NN + 3N$ Hamiltonian with $\lambda = 1.8$, 2.2, 2.5, and 3.0 fm^{-1}.

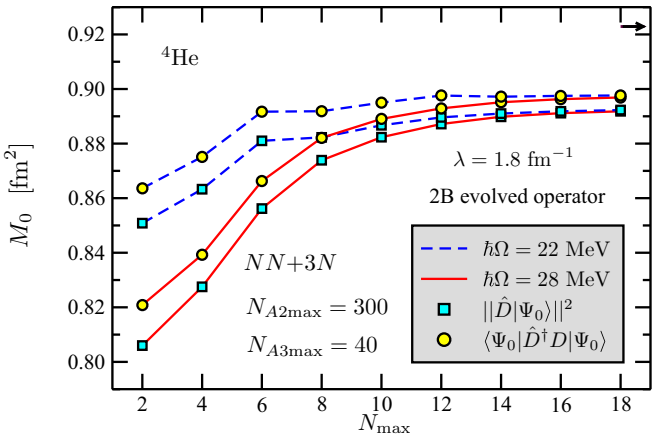

FIG. 4. (Color online) Convergence as a function of $N_{\max}$ of the 2B evolved total dipole strength, M_0, of ^{4}He computed as $||\hat{D}|\Psi_0\rangle||^2$ (squares) and $\hat{D}^\dagger\hat{D}$ (circles) for $\lambda = 1.8$ fm^{-1} and $\hbar\Omega = 22$ MeV (dashed lines) and 28 MeV (solid lines). The arrow shows the converged value of M_0 computed with the bare operator. Results were obtained using the wave function from the $NN + 3N$ Hamiltonian.

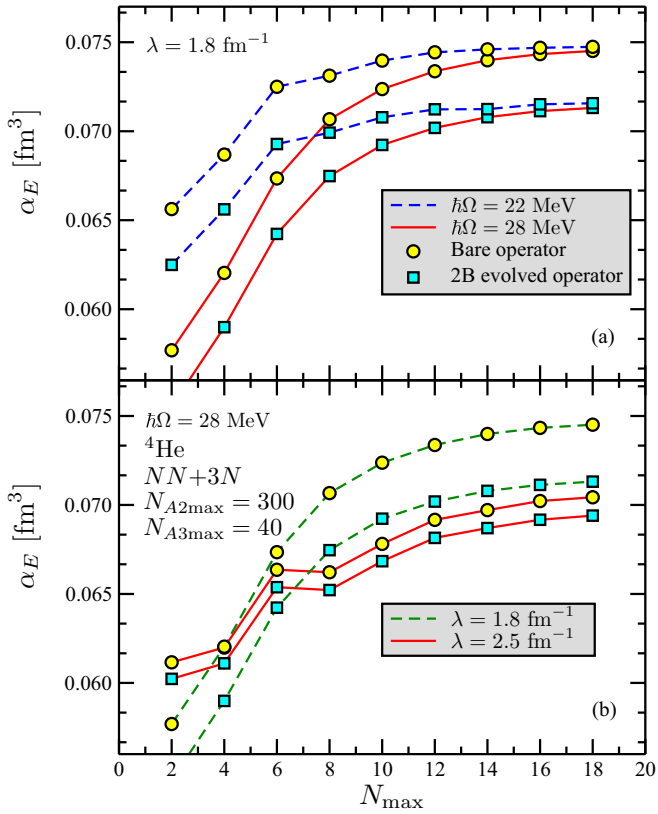

FIG. 5. (Color online) Convergence of the bare (circles) and 2B SRG evolved (squares) electric polarizability of ^{4}He as a function of $N_{\max}$ for (a) $\lambda = 1.8$ fm^{-1} with $\hbar\Omega = 22$ MeV (dashed line) and 28 MeV (solid line) and (b) with fixed $\hbar\Omega = 28$ MeV at $\lambda = 1.8$ (dashed line) and 2.5 fm^{-1} (solid line). Results were obtained using the wave function from the $NN + 3N$ Hamiltonian.

spaces reached in the present work. More interesting are the differences in the size of 2B-induced contributions for the total dipole strength calculated as $||\hat{D}|\Psi_0\rangle||^2$ versus $\langle\Psi_0|\hat{D}^\dagger\hat{D}|\Psi_0\rangle$. A somewhat larger renormalization is observed in the case of the former.

Next, in Fig. 5, we consider the electric dipole polarizability, calculated according to Eq. (15) with $M_0 = ||\hat{D}|\Psi_0\rangle||^2$. Two values of the frequency ($\hbar\Omega = 22$ and 28 MeV) and the SRG momentum scale ($\lambda = 1.8$ and 2.5 fm^{-1}) are explored for $N_{\max}$ values varying between 2 and 18. The convergence patterns obtained for the bare versus 2B evolved operator are once again very similar, although a slightly faster flattening of the curves can be observed for the latter, and the two frequencies adopted yield very similar results at $N_{\max} = 18$. As with the total dipole strength, the inclusion of the 2B evolved operator reduces the spread in the SRG momentum scale and the contribution of the 2B-induced terms is larger for $\lambda = 1.8$ fm^{-1}.

To conclude this section, we assess by means of Fig. 6 the sensitivity of the ^{4}He photoabsorption cross section, computed according to Eq. (8), to variations of the HO model-space size and frequency. The total dipole strength entering the evaluation of the LIT (12), and hence of the response function $R(\omega)$ of Eq. (9), was obtained as $M_0 = ||\hat{D}|\Psi_0\rangle||^2$ using the 2B evolved operator. Both $NN + 3N$-induced and $NN + 3N$ Hamiltonians are considered. For the sake of comparison, after being computed, all theoretical cross sections are shifted to the experimental threshold for the ^{4}He photodisintegration, $E_{\rm th} = 19.8$ MeV ($\omega \to \omega + \Delta E_{\rm th}$, with $\Delta E_{\rm th}$ being the difference of the calculated and experimental thresholds). This allows us to highlight differences beyond those occurring at the level of the ^{4}He and ^{3}H binding energies. Due to the selection rules associated with the dipole operator (10), for a given $N_{\max}$ in the $J^\pi T = 0^+0$ model space used to expand $|\Psi_0\rangle$, a complete calculation of Eq. (12) requires the expansion of the starting Lanczos vector $|\varphi_0\rangle = M_0^{-1/2}\hat{D}|\Psi_0\rangle$ over a $J^\pi T = 1^-1$ space up to $N_{\max} + 1$. This is the origin of the odd/even notation for $N_{\max}$ introduced in Fig. 6. The relative uncertainty due to the finite size of the HO space, estimated from the difference of the cross section calculated at $N_{\max} = 18/19$ and $16/17$ is largest for the $NN + 3N$ Hamiltonian, remaining below 2% above $\omega \sim 22$ MeV. At lower energies—where the cross section is smaller—the relative uncertainty grows somewhat reaching a value of ∼8% at threshold. Varying the HO frequency from 28 to 22 MeV produces results within 3%, except for energies very close to threshold. Finally, as shown in Fig. 6(b), the present $NN + 3N$-induced results are consistent with those obtained in Ref. [33] using a LS transformation of the N^{3}LO NN potential at the 3B cluster level, in which the dipole operator was not renormalized.

C. SRG resolution scale dependence

In Fig. 7, we study the dependence on the SRG evolution parameter of the ^{4}He total dipole strength and electric dipole polarizability. These results were obtained with an oscillator frequency of $\hbar\Omega = 28$ MeV and converged calculations at $N_{\max} = 18$.

The behavior of the total dipole strength as a function of λ, presented in Fig. 7(a), is consistent with that obtained in our previous study [26] of the evolution of the $\hat{D}^\dagger\hat{D}$ operator up

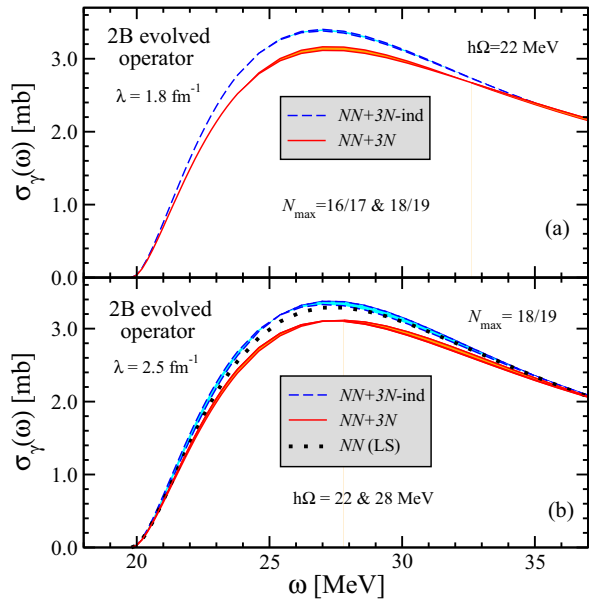

FIG. 6. (Color online) Dependence of the ^{4}He total photoabsorption cross section computed with the $NN + 3N$-induced (region delimited by dashed [blue] lines) and $NN + 3N$ (region delimited by solid [red] lines) Hamiltonians and a 2B evolved dipole operator on (a) the model-space size $N_{\max}$ at $\hbar\Omega = 28$ MeV and $\lambda = 1.8$ fm^{-1} and (b) the HO frequency $\hbar\Omega$ at $N_{\max} = 18/19$ and $\lambda = 2.5$ fm^{-1}. Also shown (dotted [black] line) is the result of the LS calculation of Ref. [33] using the N^{3}LO NN interaction.

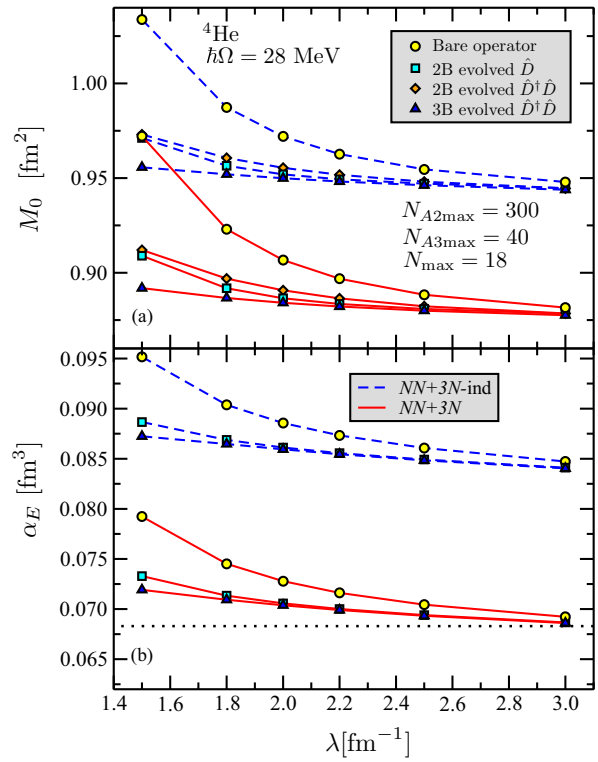

FIG. 7. (Color online) Dependence of (a) total strength of the dipole transition and (b) electric dipole polarizability on variations of the SRG flow parameter, λ, for $N_{\max} = 18$ and $\hbar\Omega = 28$ MeV, obtained using wave functions from the $NN + 3N$-induced (dashed lines) and $NN + 3N$ (solid lines) Hamiltonians along with four types of operators: bare (circles), 2B evolved $\hat{D}$ (squares), 2B evolved $\hat{D}^\dagger\hat{D}$ (diamonds), and 3B evolved $\hat{D}^\dagger\hat{D}$ (triangles). The dotted line in panel (b) indicates the evaluation of Ref. [34] based on a LS renormalization of the N^{3}LO NN plus N^{2}LO $3N$ interactions and bare dipole operator. See the text for more details.

to the 3B level. Different from that work, here we also show results obtained by computing M_0 as the norm $||\hat{D}|\Psi_0\rangle||^2$ of the 2B evolved dipole operator acting on the g.s. wave function. When using the bare operator, the observables have a significant dependence on λ, particularly at smaller values. When using the 2B evolved operators, this dependence is reduced. The difference between the bare and 2B evolved operator, which we refer to as the 2B contribution to the evolution, is larger at smaller values of λ and tends to decrease rapidly as λ increases. Further, such a 2B contribution is found to be larger when the total strength is calculated as $||\hat{D}|\Psi_0\rangle||^2$ using the 2B evolved dipole operator. This is related to the longer range of the $\hat{D}^\dagger\hat{D}$ operator compared to the dipole itself. For the time being, results for the evolution at the 3B level have been obtained only for the scalar $\hat{D}^\dagger\hat{D}$ operator [26]. The 3B contribution to the operator evolution is much smaller than the 2B contribution, establishing a hierarchy in the magnitude of the SRG-induced terms for operator evolution. Overall, the smallest spread in λ is found using the 3B evolved $\hat{D}^\dagger\hat{D}$ operator. The slight residual dependence on λ is due to the induced 4B terms that we do not take into account for these calculations.

The electric dipole polarizabilty, presented in Fig. 7(b), shows a trend similar to that of the total dipole strength. The inclusion of the 2B-induced terms of the operator provides a substantial correction to the polarizability, especially at smaller values of λ. To estimate the contribution to this observable of 3B-induced terms of the operator, in Fig. 7(b) we also show the polarizability (triangles) obtained by rescaling the 2B evolved polarizability (squares), by the ratio $\langle\Psi_0|\hat{D}^\dagger\hat{D}|\Psi_0\rangle/||\hat{D}|\Psi_0\rangle||^2$, where the $\hat{D}^\dagger\hat{D}$ operator is evolved in the $3N$ space and $||\hat{D}|\Psi_0\rangle||^2$ is evolved in the NN space. The residual dependence on λ displayed by these rescaled results comes then from 4B-induced SRG terms but also from missing 3B-induced dipole operator terms in the calculation of the Green's function, $G(E_0)$, of Eq. (15). This latter contribution is expected to be small if the Hamiltonian is evolved up to the 3B level. Also shown in the figure as a dotted line is the evaluation of Ref. [34] based on a LS renormalization of the N^{3}LO NN plus N^{2}LO $3N$ interactions and bare dipole operator.

Finally, in Fig. 8 we explore the effect of the SRG evolution of the transition operator on the ^{4}He photoabsorption cross section. This study was performed using our largest model space of $N_{\max} = 18/19$ at $\hbar\Omega = 28$ MeV and both $NN + 3N$-induced and $NN + 3N$ wave functions, varying the SRG resolution scale between 1.8 and 3.0 fm^{-1}. We choose this range of λ because previous structure calculations show that the g.s. energy is mostly independent of the transformation in this region. As shown in Fig. 8(a), when using the bare dipole operator there is a clear dependence of the cross section on λ,

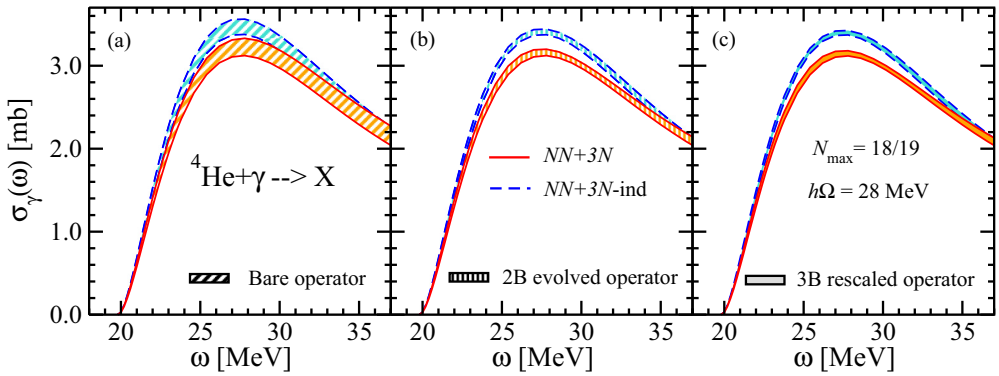

FIG. 8. (Color online) Dependence (represented as the width of the bands) on the variation of λ between 1.8 and 3.0 fm^{-1} of the ^{4}He photoabsorption cross section, $\sigma_\gamma(\omega)$, as a function of the photon energy, ω, at $N_{\max} = 18/19$ and $\hbar\Omega = 28$ MeV, using the $NN + 3N$-induced (dashed contours) and $NN + 3N$ (solid contours) wave functions. Calculations were obtained (a) with the bare dipole operator; (b) with the 2B evolved dipole operator; and (c) by rescaling the 2B evolved results by the ratio $\langle\Psi_0|\hat{D}^\dagger\hat{D}|\Psi_0\rangle/||\hat{D}|\Psi_0\rangle||^2$, with the $\hat{D}^\dagger\hat{D}$ operator evolved in the $3N$ space (3B rescaled operator, see text for details).

and the spread is slightly larger for the calculation using the $NN + 3N$ Hamiltonian. Specifically, beginning at a photon energy of 26 MeV and persisting up to the largest energy shown here, there is a spread of more than 0.2 mb between the $NN + 3N$ cross sections obtained with the smallest and largest values of λ (corresponding, respectively, to the upper and lower bounds of the shaded areas). This amounts to an effect between 6% and 11%, depending on the photon energy, which is substantially larger than our uncertainty due to the finite size of the HO model space or choice of frequency. Further, this spread is comparable to the contribution coming from the inclusion of the initial chiral $3N$ force into the Hamiltonian, which—at a given λ value—quenches the peak of the cross section by about 0.25 mb. When we evolve the dipole operator in the 2B space [see Fig. 8(b)], the spread in the cross section is a factor of 3 tighter, about 0.06 mb (between 2% and 4% in the range 24 MeV $\leqslant \omega \leqslant$ 35 MeV), and the effect of the inclusion of the initial chiral $3N$ force can be clearly singled out. To take into account 3B-induced terms of the transition operator, at least in part, the cross sections of Fig. 8(b) can be further rescaled by the ratio $\langle\Psi_0|\hat{D}^\dagger\hat{D}|\Psi_0\rangle/||\hat{D}|\Psi_0\rangle||^2$, with the $\hat{D}^\dagger\hat{D}$ operator evolved in the $3N$ space (3B rescaled operator). The result of this operation, shown in Fig. 8(c), is mainly an overall small reduction of all curves and a very minor narrowing of the spread in λ. The remaining λ dependence is due, once again, to 4B-induced SRG terms and from missing 3B-induced dipole operator terms in the calculation of the Green's function, $G(E_0)$, of Eq. (12).

D. Comparison with literature and experiment

Table I presents a summary of our results for the total dipole strength $\langle\Psi_0|\hat{D}^\dagger\hat{D}|\Psi_0\rangle$ and the electric dipole polarizability α_E obtained employing the $NN + 3N$-induced and $NN + 3N$ Hamiltonians along with the 3B evolved $\hat{D}^\dagger\hat{D}$ operator in the largest model space. For the electric polarizability, these results represent an upper bound because the effects of 3B-induced dipole operator terms in the calculation of the Green's function of Eq. (15) are still missing. Two values of λ, 1.8 and 3.0 fm^{-1}, are shown to help quantify the effect of missing induced terms. For completeness, we also show the corresponding values of the g.s. energy, E_0, and the point-proton root-mean-square radius, $\sqrt{\langle r_p^2\rangle}$, of Ref. [26], including 3B-induced terms. The error estimates of the observables are computed as the difference between the value at the largest model space, $N_{\max} = 18$, and at the next smallest model space, $N_{\max} = 16$. The present results for the g.s. energy are the same as the previous NCSM

TABLE I. Calculated ^{4}He g.s. energy E_0, point-proton root-mean-square radius $\sqrt{\langle r_p^2\rangle}$, total dipole strength $\langle\Psi_0|\hat{D}^\dagger\hat{D}|\Psi_0\rangle$, and electric dipole polarizability α_E using the using the λ = 1.8 and 3.0 fm^{-1} $NN + 3N$-induced and $NN + 3N$ Hamiltonians along with 3B evolved operators compared to results published in the literature and experiment. See the text for more details.

Interaction	λ (fm^{-1})	$E_{\text{g.s.}}$ (MeV)	$\sqrt{\langle r_p^2\rangle}$ (fm)	$\langle\Psi_0|\hat{D}^\dagger\hat{D}|\Psi_0\rangle$ (fm^2)	α_E (fm^3)
$NN + 3N$-induced	1.8	−25.325(1)	1.5231(11)	0.9520(3)	0.08647(5)
	3.0	−25.348(2)	1.5165(12)	0.9439(4)	0.08404(5)
N^{3}LO NN (LS) [33]	–	−25.39(1)	1.515(2)	0.943(1)	–
$NN + 3N$	1.8	−28.464(2)	1.4723(7)	0.8867(4)	0.07093(5)
	3.0	−28.458(3)	1.4651(5)	0.8776(5)	0.06861(5)
Evaluation (LS) [34]	–	–	–	–	0.0683(8)(14)
Expt.	–	− 28.296 [53]	1.455(7) [54]	–	0.072(4) [58]
					0.076(8) [59]

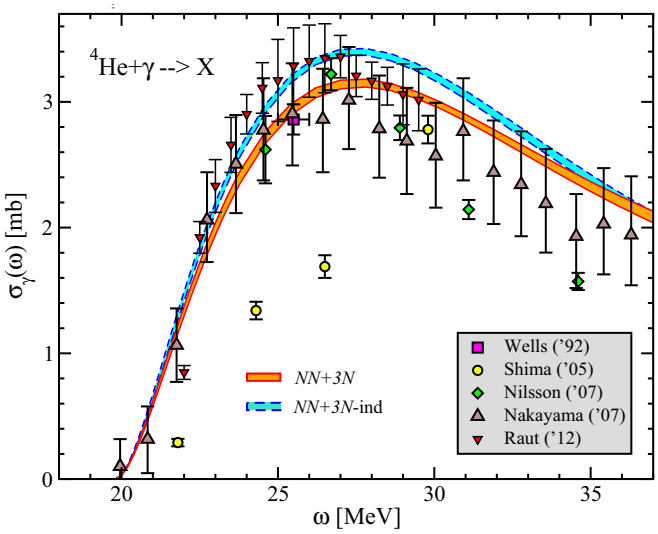

FIG. 9. (Color online) The ^{4}He photoabsorption cross section as a function of excitation energy, ω, for $NN+3N$-induced (blue dashed line) and $NN+3N$ (red solid line) interactions with a model-space truncation of $N_{\max} = 18/19$ and oscillator frequency of $\hbar\Omega = 28$ MeV. The total cross section is compared to experimental results from Wells *et al.* [60], Shima *et al.* [61], Nilsson *et al.* [62], Nakayama *et al.* [63], and Raut *et al.* [64]. See the text for more details.

calculation of Ref. [8] and those for the $NN+3N$-induced point-proton radius and total dipole strength are consistent with those obtained in Ref. [33] using a LS transformation of the N^{3}LO NN potential at the 3B cluster level, in which the operators were not renormalized. In particular, the agreement with the LS values is excellent for $\lambda = 3.0$ fm^{-1}, where the contribution of 4B-induced terms is negligible. A similar comparison for the $NN+3N$ Hamiltonian is not possible, because the results of Ref. [33] were obtained with a sightly different parametrization of the N^{2}LO 3N force. Also in very good agreement with the evaluation of Ref. [34] and with experiment is the electric dipole polarizability computed with the $NN+3N$ interaction.

For completeness, in Fig. 9, we compare our results for the ^{4}He photoabsorption cross section of Fig. 8(c) to experimental data in the region $\omega < 40$ MeV, where corrections to the unretarded dipole approximation used here to describe the photodisintegration process are expected to be largely negligible. As for the electric polarizability, the present results represent an upper bound due to the missing effect of 3B-induced dipole operator terms in the calculation of the Green's function of Eq. (15). The photodisintegration of ^{4}He has been the subject of many experiments (see, e.g., Refs. [61–64] for the most recent ones) and has already been investigated in *ab initio* calculations including 3N forces [33,65]. The results obtained here with the $NN+3N$-induced Hamiltonian are close to the recent coupled cluster calculation of Ref. [66], using the bare N^{3}LO potential. Different from Ref. [33], here the $NN+3N$ results have been obtained starting from the N^{2}LO 3N force of Ref. [49]. Therefore, the two calculations cannot be compared directly. Nevertheless, the overall picture drawn by the present study is not very dissimilar from that of Ref. [33] or Ref. [65]. In particular, although the inclusion of the 3N force and the evolved dipole operator produces a seemingly improved agreement with experiment, the considerable scatter of the experimental data in the peak region continues to prevent a definitive conclusion concerning the quality of the interactions used. Note that in Fig. 9 we estimated the total cross section from the ^{4}He(γ,n) measurements of Ref. [62] by assuming $\sigma_\gamma(\omega) \approx 2\sigma_{\gamma,n}(\omega)$ and that from the ^{4}He$(\gamma,p)^3$H of Ref. [64] by assuming $\sigma_\gamma(\omega) \approx \sigma_{\gamma,p}(\omega) + \sigma_{\gamma,p}(\omega + 0.5$ MeV).

IV. CONCLUSION

We have, for the first time, SRG evolved the dipole operator in the 2B space and computed the total strength of the dipole transition, the electric dipole polarizability, and the total photoabsorption cross section of ^{4}He. Because the dipole operator acts primarily at long range, we see little change in the convergence properties of these observables over using the bare operator.

For all three observables, there is a significant reduction of the dependence on the SRG evolution parameter when evolving the dipole operator in the 2B space. Generally, this reduction is on the order of the effect of including the 3N force. So although the reduction is relatively small in magnitude, its effects are not negligible. Any residual dependence on λ in our calculations is due to the induced 3B and 4B terms that we do not take into account. Based on our experience with calculations of energies and radii, these higher-order contributions should be smaller than the 2B contributions to the evolution. Consistently evolving operators is important for maintaining the rigorous nature of *ab initio* calculations based on SRG evolved Hamiltonians. Although we have, so far, been concerned with long-range operators for which the principle benefit of the evolution is the reduced dependence on λ, there are other shorter-range operators (e.g., β- or $\beta\beta$-decay operators including 2B currents) for which the SRG transformation will likely have a larger effect, including on the convergence pattern. At the same time, a study of the evolution of both long- and short-range operators in heavier nuclei will be needed to clarify whether the reduction in λ dependence and/or improvement in convergence rates are substantial enough to motivate the extra step of systematically evolving operators.

Future work will include evolving the dipole operator, and other nonscalar operators, in the 3B space. This will allow us to investigate the 3B and 4B contributions to the evolution of these operators in the $A = 4$ system. We also plan to extend these calculations to heavier systems (e.g., up to $A = 12$), where it is advantageous to work with single-particle Slater determinant basis states. We will do this by transforming our 2B and, eventually, 3B nonscalar operators, presently in a translationally invariant Jacobi-coordinate basis, into matrix elements over Slater determinate basis states.

ACKNOWLEDGMENTS

This work was performed in part under the auspices of the U.S. Department of Energy by the Lawrence Livermore

National Laboratory (LLNL) under Contract No. DE-AC52-07NA27344. This material is based upon work supported by the U.S. Department of Energy, Office of Science, Office of Nuclear Physics, under Awards No. DE-FG02-96ER40985 and No. DE-FC02-07ER41457 as well as under Work Proposal No. SCW1158. Additional support came from the Natural Sciences and Engineering Research Council of Canada (NSERC) under Grant No. 401945-2011. TRIUMF receives funding via a contribution through the Canadian National Research Council. Computing support came from the LLNL institutional Computing Grand Challenge program. Additional resources came from the Computational Science Research Center and the Department of Physics at San Diego State University.

[1] S. Okubo, Prog. Theo. Phys. **12**, 603 (1954).
[2] D. C. Zheng, B. R. Barrett, L. Jaqua, J. P. Vary, and R. J. McCarthy, Phys. Rev. C. **48**, 1083 (1993).
[3] I. Stetcu *et al.*, Nucl. Phys. A. **785**, 307 (2007).
[4] A. Nogga, P. Navrátil, B. R. Barrett, and J. P. Vary, Phys. Rev. C **73**, 064002 (2006).
[5] P. Navrátil, J. P. Vary, and B. R. Barrett, Phys. Rev. C **62**, 054311 (2000).
[6] N. Barnea, W. Leidemann, and G. Orlandini, Phys. Rev. C **61**, 054001 (2000).
[7] N. Barnea, W. Leidemann, and G. Orlandini, Nucl. Phys. A **693**, 565 (2001).
[8] E. D. Jurgenson, P. Navrátil, and R. J. Furnstahl, Phys. Rev. C **83**, 034301 (2011).
[9] R. Roth, J. Langhammer, A. Calci, S. Binder, and P. Navrátil, Phys. Rev. Lett. **107**, 072501 (2011).
[10] I. Stetcu and J. Rotureau, Prog. Part. Nucl. Phys. **69**, 182 (2013).
[11] R. J. Furnstahl and K. Hebeler, Rep. Prog. Phys. **76**, 126301 (2013).
[12] S. K. Bogner, R. J. Furnstahl, and R. J. Perry, Phys. Rev. C **75**, 061001 (2007).
[13] E. D. Jurgenson, P. Navrátil, and R. J. Furnstahl, Phys. Rev. Lett. **103**, 082501 (2009).
[14] R. Roth, S. Binder, K. Vobig, A. Calci, J. Langhammer, and P. Navrátil, Phys. Rev. Lett. **109**, 052501 (2012).
[15] N. M. Dicaire, C. Omand, and P. Navrátil, Phys. Rev. C **90**, 034302 (2014).
[16] K. A. Wendt, Phys. Rev. C **87**, 061001(R) (2013).
[17] K. Tsukiyama, S. K. Bogner, and A. Schwenk, Phys. Rev. Lett. **106**, 222502 (2011).
[18] H. Hergert, S. K. Bogner, S. Binder, A. Calci, J. Langhammer, R. Roth, and A. Schwenk, Phys. Rev. C **87**, 034307 (2013).
[19] G. Hupin, S. Quaglioni, and P. Navrátil, Phys. Rev. C **90**, 061601 (2014).
[20] G. Hupin, J. Langhammer, P. Navrátil, S. Quaglioni, A. Calci, and R. Roth, Phys. Rev. C **88**, 054622 (2013).
[21] J. Langhammer, P. Navrátil, S. Quaglioni, G. Hupin, A. Calci, and R. Roth, Phys. Rev. C **91**, 021301(R) (2015).
[22] K. Suzuki and S. Y. Lee, Prog. Theor. Phys. **64**, 2091 (1980).
[23] K. Suzuki, Prog. Theor. Phys. **68**, 1999 (1982).
[24] I. Stetcu, B. R. Barrett, P. Navrátil, and J. P. Vary, Phys. Rev. C **71**, 044325 (2005).
[25] E. R. Anderson, S. K. Bogner, R. J. Furnstahl, and R. J. Perry, Phys. Rev. C **82**, 054001 (2010).
[26] M. D. Schuster, S. Quaglioni, C. W. Johnson, E. D. Jurgenson, and P. Navrátil, Phys. Rev. C **90**, 011301(R) (2014).
[27] E. Epelbaum, H.-W. Hammer, and U.-G. Meißner, Rev. Mod. Phys. **81**, 1773 (2009).
[28] R. Machleidt and D. R. Entem, Phys. Rep. **503**, 1 (2011).
[29] P. Navrátil, G. P. Kamuntavičius, and B. R. Barrett, Phys. Rev. C **61**, 044001 (2000).
[30] V. D. Efros, W. Leidemann, and G. Orlandini, Phys. Lett. B **338**, 130 (1994).
[31] V. D. Efros, W. Leidemann, G. Orlandini, and N. Barnea, J. Phys. G **34**, R459 (2007).
[32] B. Podolsky, Proc. Natl. Acad. Sci. USA **14**, 253 (1928).
[33] S. Quaglioni and P. Navrátil, Phys. Lett. B **652**, 370 (2007).
[34] I. Stetcu, S. Quaglioni, J. L. Friar, A. C. Hayes, and P. Navrátil, Phys. Rev. C **79**, 064001 (2009).
[35] P. Navrátil and W. E. Ormand, Phys. Rev. Lett. **88**, 152502 (2002).
[36] P. Navrátil and W. E. Ormand, Phys. Rev. C **68**, 034305 (2003).
[37] C. Lanczos, J. Res. Natl. Bur. Stand. **45**, 255 (1950).
[38] R. Haydock, J. Phys. A: Math. Nucl. Gen. **7**, 2120 (1974).
[39] W. C. Haxton, K. M. Nollett, and K. M. Zurek, Phys. Rev. C **72**, 065501 (2005).
[40] S. K. Bogner, R. J. Furnstahl, and A. Schwenk, Prog. Part. Nucl. Phys. **65**, 94 (2010).
[41] F. Wegner, Ann. Phys. **506**, 77 (1994).
[42] W. Li, E. R. Anderson, and R. J. Furnstahl, Phys. Rev. C **84**, 054002 (2011).
[43] J. S. Levinger and H. A. Bethe, Phys. Rev. **78**, 115 (1950).
[44] V. D. Efros, W. Leidemann, and G. Orlandini, Few-Body Syst. **26**, 251 (1999).
[45] D. Andreasi, W. Leidemann, C. Reiß, and M. Schwamb, Eur. Phys. J. A **24**, 361 (2005).
[46] M. A. Marchisio, N. Barnea, W. Leidemann, and G. Orlandini, Few-Body Syst. **33**, 259 (2003).
[47] D. R. Entem and R. Machleidt, Phys. Rev. C **68**, 041001 (2003).
[48] P. Navrátil, Few-Body Syst. **41**, 117 (2007).
[49] D. Gazit, S. Quaglioni, and P. Navrátil, Phys. Rev. Lett. **103**, 102502 (2009).
[50] R. Roth, A. Calci, J. Langhammer, and S. Binder, Phys. Rev. C **90**, 024325 (2014).
[51] E. Anderson, S. K. Bogner, R. J. Furnstahl, E. D. Jurgenson, R. J. Perry, and A. Schwenk, Phys. Rev. C **77**, 037001 (2008).
[52] S. A. Coon and M. K. G. Kruse, in *Proceedings of International Workshop on Nuclear Theory in the Supercomputing Era (NTSE-2013), Ames, Iowa, 2013*, edited by A. Shirokov and A. Mazur (Pacific National University, Khabarovsk, 2014), pp. 314–324.
[53] D. R. Tilley, H. R. Weller, and G. M. Hale, Nucl. Phys. A **541**, 1 (1992).
[54] The experimental value of the point-proton radius is deduced from the measured ^{4}He charge radius, $\sqrt{\langle r_c^2\rangle}$=1.673(1) fm [55], the proton charge radius, $\sqrt{\langle R_p^2\rangle}$=0.895(18) fm [56], and the neutron mean-square-charge radius, $\langle R_n^2\rangle = 0.120(5)\,\mathrm{fm}^2$ [57].

[55] E. Borie and G. A. Rinker, Phys. Rev. A **18**, 324 (1978).
[56] I. Sick, Phys. Lett. B **576**, 62 (2003).
[57] S. Kopecky, P. Riehs, J. A. Harvey, and N. W. Hill, Phys. Rev. Lett. **74**, 2427 (1995).
[58] J. L. Friar, Phys. Rev. C **16**, 1540 (1977).
[59] K. Pachucki and A. M. Moro, Phys. Rev. A **75**, 032521 (2007).
[60] D. P. Wells *et al.*, Phys. Rev. C **46**, 449 (1992).
[61] T. Shima *et al.*, Phys. Rev. C **72**, 044004 (2005).
[62] B. Nilsson *et al.*, Phys. Rev. C **75**, 014007 (2007).
[63] S. Nakayama *et al.*, Phys. Rev. C **76**, 021305(R) (2007).
[64] R. Raut, W. Tornow, M. W. Ahmed, A. S. Crowell, J. H. Kelley, G. Rusev, S. C. Stave, and A. P. Tonchev, Phys. Rev. Lett. **108**, 042502 (2012).
[65] D. Gazit, S. Bacca, N. Barnea, W. Leidemann, and G. Orlandini, Phys. Rev. Lett. **96**, 112301 (2006).
[66] S. Bacca, N. Barnea, G. Hagen, M. Miorelli, G. Orlandini, and T. Papenbrock, Phys. Rev. C **90**, 064619 (2014).